Applied Materials Today 29 (2022) 101567

Contents lists available at ScienceDirect

Applied Materials Today

journal homepage: www.elsevier.com/locate/apmt

Scaling up anodic TiO_2 nanotube layers – Influence of the nanotube layer thickness on the photocatalytic degradation of hexane and benzene

Hanna Sopha [a,b], Michal Baudys [c], Ludek Hromadko [a,b], Miloslav Lhotka [c], David Pavlinak [b], Josef Krysa [c], Jan M. Macak [a,b,*]

[a] Center of Materials and Nanotechnologies, Faculty of Chemical Technology, University of Pardubice, Nam. Cs. Legii 565, 53002 Pardubice, Czech Republic
[b] Central European Institute of Technology, Brno University of Technology, Purkyňova 123, 612 00 Brno, Czech Republic
[c] Department of Inorganic Technology, University of Chemistry and Technology Prague, Technicka 5, 166 28 Prague, Czech Republic

ARTICLE INFO

Keywords:
TiO_2 nanotube layers
anodization
large areas
upscaling
gasphase photocatalysis

ABSTRACT

In this work, the preparation of homogenous TiO_2 nanotube (TNT) layers with different thicknesses via anodization on Ti substrates with a large geometrical area of two times 5 cm x 10 cm (i.e. both sides of the Ti substrate) is shown for the first time. TNT layers with four different thicknesses of ~0.65 μm, ~1 μm, ~7 μm, and ~14 μm were prepared with excellent conformality and homogeneity over the anodized area. These TNT layers were successfully employed as photocatalysts for the degradation of hexane and benzene as model compounds in the gas phase under ISO standards, showing an increase of the conversion for both model compounds with the TNT layer thickness. While a stable hexane conversion was observed for all TNT layers during the measuring time of three hours, in case of benzene degradation an initial conversion decrease was monitored before the conversion stabilized. Despite this trend, SEM and XPS analyses did not reveal any significant amount of reaction products on the TNT layer surface.

Introduction

TiO_2 is considered as one of the most promising photocatalysts due to its excellent photocatalytic performance, its high stability, non-toxicity, and availability, though it is just active under UV irradiation due its wide band gap of 3.2 eV for anatase phase and ~3.0 eV for rutile phase [1–4]. The photocatalytic activity stems from the formation of electron-hole pairs upon light illumination resulting in the creation of highly reactive radicals which can be used for the decomposition of pollutants, in the liquid as well as in the gas phase [5–7]. Rationally, a higher surface area of the photocatalyst will lead to an increase of electron-hole pairs formed and thus to higher pollutant degradation rates. Therefore, within the last two decades several different TiO_2 nanostructures have been prepared and employed for photocatalysis, such as TiO_2 nanoparticles [6,8–10], TiO_2 nanorods [10–12], TiO_2 nanowires [13,14], or TiO_2 nanotubes [7–16]. Due to their extremely high surface area inside and outside their walls, particularly TiO_2 nanotubes are of high interest.

TiO_2 nanotubes can be produced by a variety of different approaches [17,18], among which the use of electrochemical anodization belongs to the most widely explored. The advantage of anodic over TiO_2 nanotubes prepared by other methods is that anodic TiO_2 nanotubes grow vertically on a Ti substrate with the nanotube openings on the top and closed nanotube bottoms adhered to the Ti substrate. Thus, no further immobilization on a substrate with a binder is needed. Such TiO_2 nanotube layers (TNT layers) are highly ordered, resulting in a straight diffusion way [19,20]. Additionally, if needed, the TNT layers can be removed from the underlying Ti substrate and used as powders [21]. Another advantage is the control of nanotube layer thickness and nanotube diameter by adjusting anodization electrolyte, potential, and time [18].

Many reports on the use of anodic TNT layers for photocatalytic degradation of pollutants can be found in the literature, however, the majority of these reports is still on photocatalytic degradation of pollutants in the liquid phase [15–18]. Reports on gas phase photocatalysis are available but still scarce, reporting on the degradation of different gaseous pollutants (e.g. toluene [5–23], benzene [5], 2,3-butanedione [24], hexane [25,26], NO_x [27,28] or acetaldehyde [29]) employing TNT layers of different length [5–31], or different light intensity [22].

Nevertheless, in all these reports TNT layers on the lab scale were used with geometric surface areas up to ~10 cm^2 [5,27]. Only two publications from our team can be found in the literature, dealing with

* Corresponding author.
E-mail address: jan.macak@upce.cz (J.M. Macak).

https://doi.org/10.1016/j.apmt.2022.101567
Received 16 March 2022; Received in revised form 24 May 2022; Accepted 16 June 2022
Available online 2 July 2022

Table 1
Dimensions and anodization conditions of the employed TNT layers.

Thickness	Inner diameter	Aspect ratio	Electrolyte	Anodization potential	Anodization time	Cathode
~0.65 µm	~55 nm	~12	270 mM NH_4F, 50 vol% H_2O, glycerol	20 V	100 min	Pt-foil
~1 µm	~75 nm	~13	270 mM NH_4F, 50 vol% H_2O, glycerol	20 V	100 min	Ti-foil
~7 µm	~160 nm	~44	150 mM NH_4F, 10 vol% H_2O, ethylene glycol	80 V	4 h	Ti-foil
~14 µm	~110 nm	~127	170 mM NH_4F, 1.5 vol% H_2O, ethylene glycol	60 V	4 h	Ti-foil

the use of TNT layers grown on planar Ti substrates for the gas phase photocatalysis with larger geometric area (50 cm^2) under ISO standards [25,26]. Additionally, one publication on the use of an anodized Ti mesh with the same geometric area for NO_x oxidation exists [28]. The reason for this limited literature lays in difficulties appearing when anodizing large Ti substrates: due to high currents flowing between the electrodes, the electrolyte heats up and there is a high possibility of dielectric breakdown to occur [25,32,33]. To circumvent this problem, different approaches exist. For instance, Lincho et al. carried out anodization in electrolytes with a volume of 8 L at a relatively low potential of 40 V for 1 h to avoid high increase of the electrolyte temperature [34]. Other approaches include intensive cooling of the electrolytes before and during the anodization process [25,35], using low anodization potentials [35,36] or using short anodization times [37]. The key is to find anodization conditions, including electrolyte temperature and composition, anodization potential and anodization time, in which the increase in electrolyte temperature is only moderate and the dielectric breakdown is avoided.

In this work, for the best of our knowledge, we demonstrate for the first time the preparation of TNT layers with a large geometric area of two times 5 cm x 10 cm with different TNT layer dimensions, i.e. TNT layer thickness and nanotube diameter, received by anodization at potentials up to 80 V and anodization times up to 4 h. All TNT layers are very homogenous in layer thickness and diameter over the whole geometric surface area. These TNT layers were further employed for the photocatalytic degradation of hexane and benzene in the gas phase under ISO standards. The results are correlated with the specific surface area obtained from Kr isotherms by using Brunauer-Emmett-Teller (BET) evaluation.

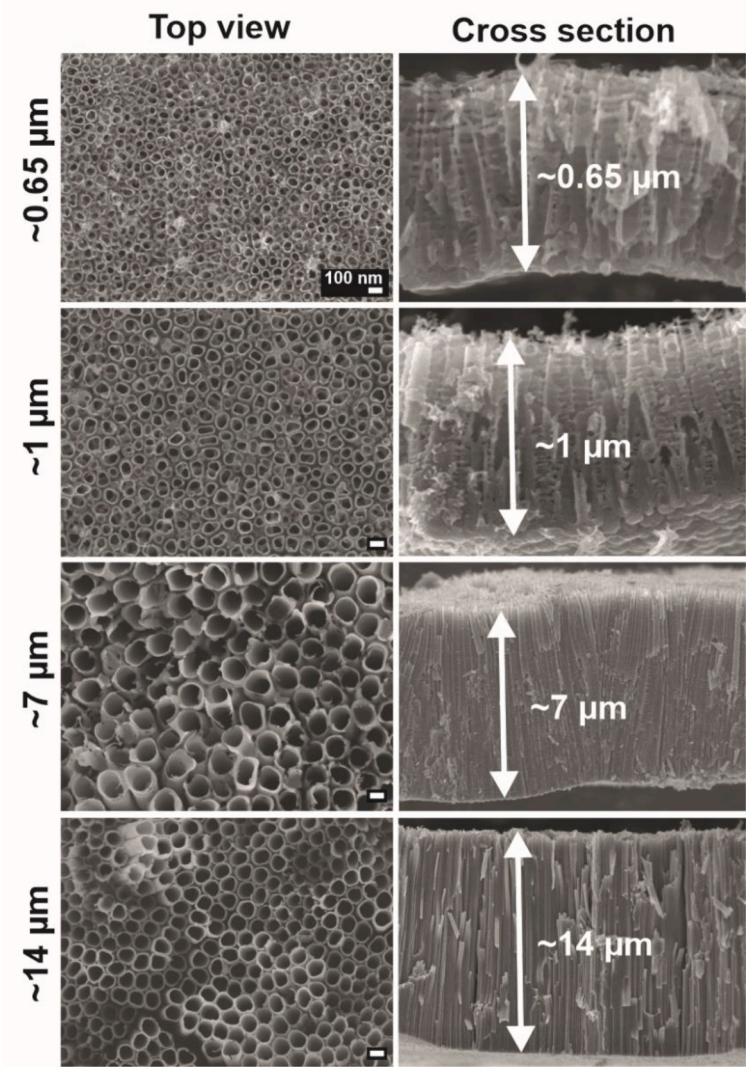

Fig. 1. SEM images of the four different TNT layers prepared with average layer thicknesses of ~0.65 µm, ~1 µm, ~7 µm, and ~14 µm.

Experimental

TNT layers were produced by anodization as described below. Ti foils (Sigma-Aldrich, 127μm thick) were cut to a size of 5 cm (width) x 12 (height) cm and immersed into the electrolyte using a crocodile clip so that 10 cm of height were soaked and 2 cm were used for the clip. It must be noted that both sides of the Ti foils were anodized during the process, making an anodized area of 100 cm^2. The backsides of the Ti foils were not masked during the anodization to avoid any contamination of the electrolytes. Before anodization the Ti foils were cleaned via sonication in isopropanol and acetone for 1 min each, rinsed with isopropanol and dried in air.

Anodization was carried out in a beaker containing the electrolyte (~700 ml) which was cooled to 10°C in case of ethylene glycol-based electrolytes and to 16°C in case of glycerol-based electrolytes using a thermostat before and during anodization. A high voltage potentiostat (PGU-200V, IPS Elektroniklabor GmbH) was used to apply a potential. The Ti foils were used as anode. As cathode either a thick Ti foil (Sigma-Aldrich, 250μm thick) of the same size, i.e. 5 cm x 10 cm, or a Pt foil of the size 1 × 2 cm^2 (in case of 0.65 μm thick TNT layers with a nanotube diameter of ~55 nm) were employed. TNT layers with four different nanotube dimensions were prepared. The approximate TNT dimensions and exact anodization conditions are given in Table 1. Before use, the TNT layers were annealed in a muffle oven at 400°C for one hour using a heating rate of 2.1°C min^{-1} to convert the amorphous TNT layers to anatase phase.

Texture analysis was carried out using the Brunauer-Emmett-Teller (BET) model. The specific surface area (S_{BET}) was measured using the krypton (purity 4.0) sorption method (ASAP 2020, Micromeritics, USA). The samples were degassed at 200°C for 12 hours prior to measurement. The equilibration time in between the measurement steps was 20 s.

A field-emission scanning electrode microscope (SEM, JEOL JSM 7500F) was used to characterize the surface morphology of the TNT layers. TNT layer dimensions (i.e. nanotube diameter and layer thickness) were evaluated using proprietary Nanomeasure software.

X-ray diffraction (XRD) measurements (Panalytical Empyrean) were carried out at 45 kV using a Cu X-ray tube and a scintillation detector Pixcel3D.

The gas phase photocatalysis set-up was built according to ISO standards (ISO 22197) with a photocatalyst area of 50 cm^2. A scheme of the set-up is shown in Fig. S1 and in our previous publication [25]. Two different model gases were employed for degradation, namely hexane and benzene, as examples for aliphatic and aromatic hydrocarbons. For the experiments, a calibrated gas mixture of 100 ppm hexane or benzene in N_2 (Linde gas) was the pollutant source and diluted with humidified air to a final concentration of 5 ppm admitted to the reactor with a flow rate of 1 L/min. In the reactor the relative humidity (RH) was set to 50 %. The gas mixture was analyzed using a gas chromatograph equipped with a flame ionization detector (GC 7890B (Agilent) with capillary column HP Plot U (15 × 0.25) Agilent).

The composition of the TNT layers after their use for the photocatalytic degradation of benzene was determined by X-ray photoelectron spectroscopy (XPS) (AXIS SupraTM, Kratos) using a monochromatic Al Ka (1486.7 eV) source. The binding energy scale was referenced to adventitious carbon (284.8 eV). The quantitative analysis was carried out using the elemental sensitivity factors provided by the manufacturer. Evaluation was performed with Casa XPS software.

Results and Discussion

Four TNT layers on Ti foils with a geometric area of two times 5 cm x 10 cm, i.e. TNT layers on both sides of the Ti foils, with different dimensions were employed in this study, as mentioned in Table 1. Fig. 1 shows SEM images of these TNT layers. To prove the homogeneity of the TNT layers and avoid any concerns about dimensional fluctuations and differences at different places of the layers, proper statistics were carried out on all layers. Measurements of the layer thicknesses were carried out at seven different places along each layer and diameters were measured on four different places. On each place at least four images were used to evaluate the layer thickness and at least five images were evaluated to determine the diameter of the nanotubes. A scheme of the TNT layers showing the places where SEM images were taken is depicted in Fig. S2. Exact statistics for all four different TNT layers on the frontside of the Ti foils are shown in Tables S1-S4. As one can see, for all TNT layers very homogenous layer thicknesses and diameters were found. The little decrease in layer thickness on the lower part as well as a little increase on the upper part of the TNT layers can be explained by a more effective cooling of the electrolyte towards the bottom of the electrochemical cell compared to the top of the cell [38]. This is because the cooling coil is fully immersed in the electrolyte, however, the air above the electrolyte is not cooled. The TNT layer dimensions were also stochastically evaluated on the backside of the Ti foils with the values given in Tables S1-S4. With exception of the thickness of the ~14 μm thick TNT layers, the TNT layer thicknesses and nanotube diameters on the backside of the Ti foils are comparable with the ones measured at the frontside. Even though the electrical field on the backside of the Ti foils must be different than on the frontside, the TNT dimensions are comparable. In case of the very thick TNT layers, however, for the case that both sides of the Ti foils should be used for an application, an anodization using a cylindrical counter electrode might be of advantage to achieve similar dimensions on both sides.

It must be noted here that the thickness of the TNT layers is mainly affected by following four parameters: the electrolyte composition and temperature, the anodization potential and time. These parameters must be carefully optimized for a successful anodization of large area Ti substrates, i.e. to avoid dielectric breakdown, which occurs especially when high current densities are operative during anodization. However, all these parameters go hand in hand and influence each other and therefore need to be optimized for every electrolyte separately.

Considering the electrolyte composition, one must keep in mind that the electrolyte composition changes with every anodization run. This translates to lower current densities in older (i.e. more often used) electrolytes than in fresh ones [33,39]. The rate of electrolyte aging, however, is as well influenced by the laboratory humidity as ethylene glycol is hygroscopic. Thus, in laboratories with higher relative humidity the electrolytes age differently (with the assumption of operating with open electrochemical cells). For the study herein, we used fresh glycerol-based electrolytes as low anodization potentials were applied, but the ethylene glycol-based electrolytes were aged before their use. Thus, the electrolyte for ~7 μm thick TNT layers was used for 112 h for the anodization small area Ti substrates at 100 V, and the electrolyte for ~14 μm thick TNT layers was used for 36 h for the anodization small area Ti substrates at 60 V before the anodization of large Ti foils.

The anodization potential has a strong influence on the received current densities and its upper limit depends strongly on the electrolyte composition. Thus, for older electrolytes higher potentials can be applied without the occurrence of dielectric breakdown.

Additionally, electrolyte temperature plays a role by affecting the growth rate of the TNT layers [38]. This means that higher electrolyte temperatures result in higher TNT layer growth rates and thus in thicker TNT layers during a constant anodization time. However, higher electrolyte temperatures also increase the possibility of the occurrence of dielectric breakdown during the anodization process [25–33].

The electrolyte temperature can be influenced by effective cooling before and during the anodization process. Nevertheless, it is also strongly influenced by the current flowing between the electrodes during anodization, meaning that higher currents increase the electrolyte temperature. This limits the size of the Ti foil to be anodized as well as the applied potential, as higher potentials lead to higher currents. Thus, to receive homogenous and thick TNT layers on large areas without dielectric breakdown, a balance must be found between the electrolyte age and composition, applied potential, cooling and the Ti foil size. This

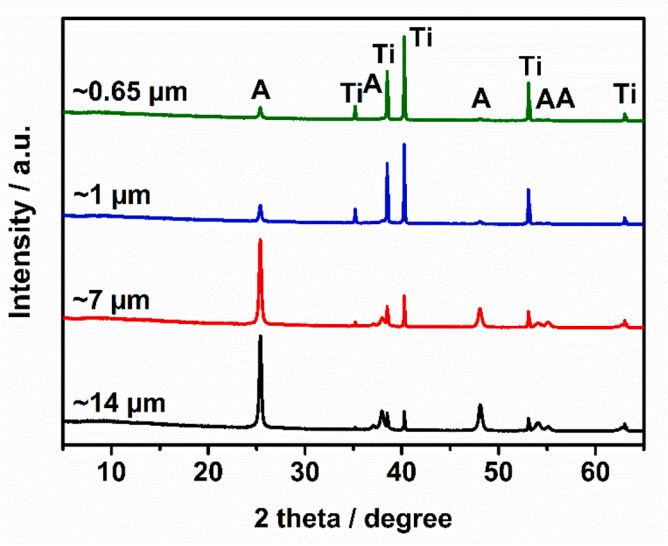

Fig. 2. XRD patterns of the annealed TNT layers of different thicknesses. A – anatase, Ti – titanium.

Table 2
Crystallite sizes, porosity, and BET specific surface areas measured using Kr for all TNT layers.

TNT layer thickness / µm	Crystallite size / Å	Porosity	S_{BET} / m^2 g^{-1}	Areal S_{BET} / cm^2 cm^{-2}
~0.65	427	0.56	44	44.4
~1	458	0.65	50	55.5
~7	456	0.76	44	260
~14	430	0.76	50	675

balance has to be optimized for each electrolyte separately, as these parameters influence each other. This limits the TNT layer thickness on such large Ti foils as used herein – 5 cm x 10 cm anodized on both sides – to ~14 µm yet.

Before further use, the as-prepared amorphous TNT layers were annealed at 400°C for 1 h. As shown in Fig. 2 all annealed TNT layers revealed anatase phase. The Ti signals stem from the underlying Ti substrates. Rationally, these Ti signals are higher for the thinner than for the thicker TNT layers while anatase signals show a higher intensity for thicker TNT layers due to the more or less equal X-ray penetration depth for all TNT layers. The crystallite sizes of anatase were calculated for all TNT layers using Scherrer equation [40] and the values are given in Table 2. As can be seen, the crystallite sizes of all TNT layers are very similar and not influenced by the TNT layer thickness or the anodization conditions.

The specific surface areas for the TNT layers were evaluated using Kr isotherms. Frequently, N_2 is used as adsorbate. For low surface areas, however, more accurate values are usually obtained when using Kr instead of N_2 [41] due to the lower vapor pressure of Kr at the adsorption measurement temperature of 77 K compared to N_2. The Kr adsorption isotherms are shown in Fig. 3. The specific surface areas per mass and per area of each TNT layer are given in Table 2.

As the TNT layers were composed of anatase TiO_2 and annealed at the same temperature, the specific surface area per mass is very similar for all TNT layers. However, naturally the specific surface area per geometric area increases with TNT layer thickness as the mass per cm^2 increases. Thus, the specific surface area per geometric area increases from ~44 cm^2 cm^{-2} for the thinnest TNT layer to ~675 cm^2 cm^{-2} for the thickest one. Obviously, the increase of the specific surface area per area is not linear with the TNT layer thickness. Therefore, the porosity of the TNT layers was estimated using the following equation [42] and the values are given in Table 2:

$$P = 1 - \frac{2\pi w(w + D)}{\sqrt{3}(D + 2w)^2} \quad (1)$$

with w being the wall thickness and D the inner diameter of the nanotubes.

Thus, the non-linear increase can be explained by a difference in porosity of the TNT layers due to variations in nanotube diameter and wall thickness, as can be seen in Fig. 1, Table 1 and Tables S1-S4.

Finally, the TNT layers with different thicknesses were used for photocatalytic application in the gas phase under ISO standards.

Fig. 4 shows the gas phase photocatalytic results for the degradation of hexane and benzene as model pollutants of the aliphatic and aromatic nature, respectively. For both compounds the same trend can be observed, namely an increase in the conversion with increase of the TNT layer thickness and specific surface area per geometric area. For the two thinnest TNT layers the conversion of each compound was almost identical. This can be explained with a very similar specific surface area per geometric area. For the two thicker TNT layers with ~7 µm and ~14

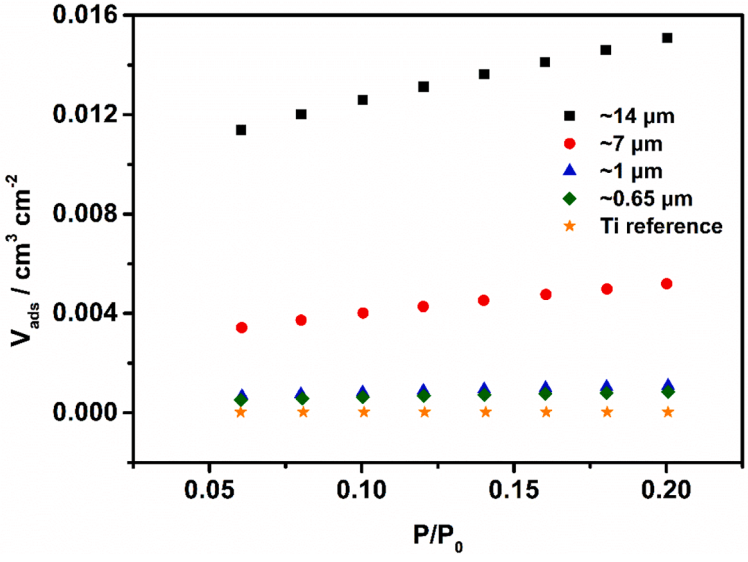

Fig. 3. Krypton adsorption isotherms for TNT layers of all thicknesses.

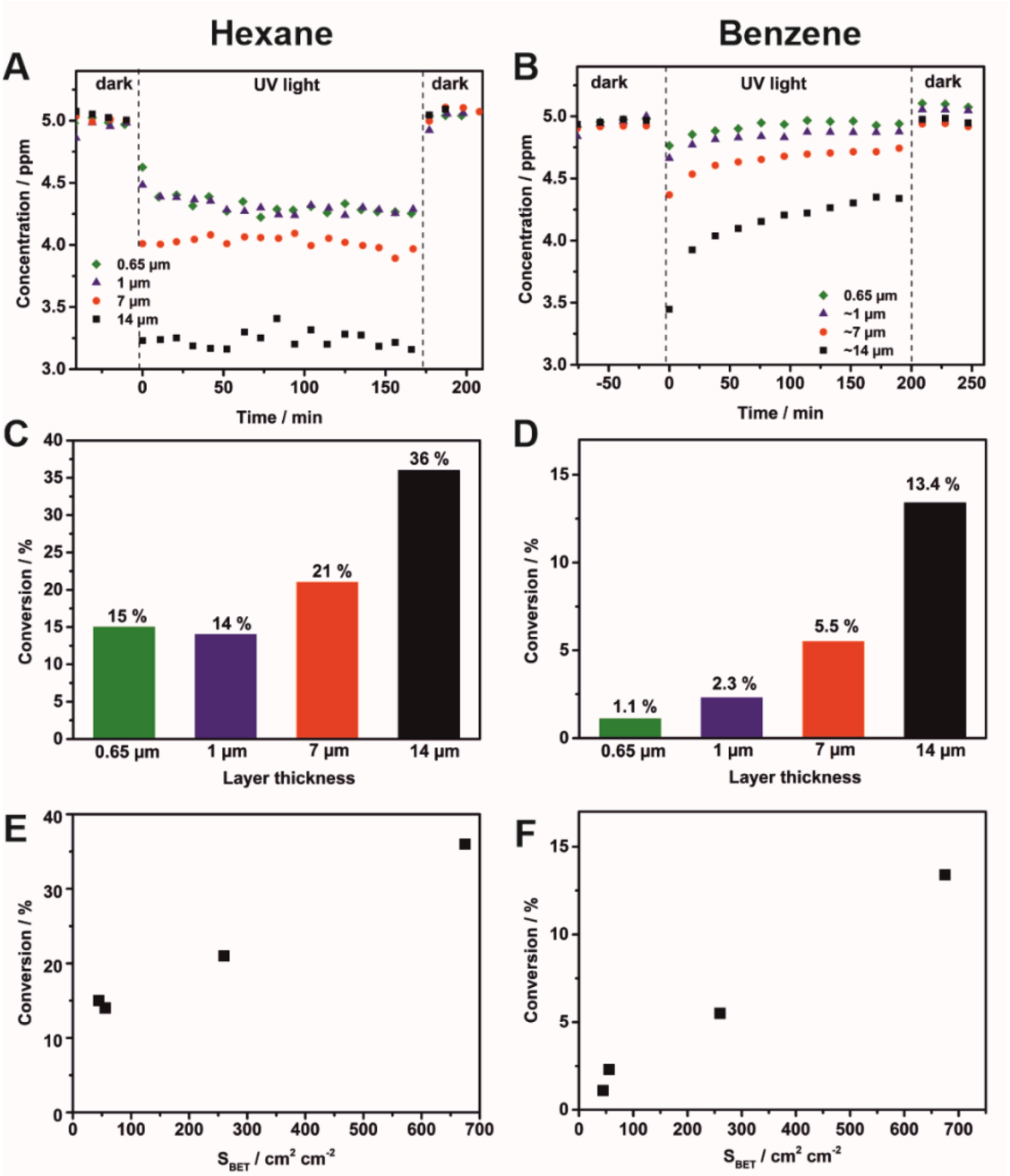

Fig. 4. Gas phase photocatalysis under ISO standard (ISO 22197): Changes in the concentration of hexane (A) and benzene (B), conversion of hexane (C) and benzene (D) for TNT layers with different thicknesses and the dependence of hexane (E) and benzene (F) conversion upon the specific surface area per area TNT layer.

µm, however, the differences are more pronounced. This indicates that at least in case of the 7 µm thick TNT layers the whole surface area of the TNT layers is used, from the top to the bottom of the nanotubes with the UV light and pollutant compounds entering the depth of the TNT layers. Additionally, a significant increase in photocatalytic conversion was found when the TNT layer thickness was increased from 7 µm to 14 µm, indicating that the UV light penetration and pollutant diffusion depth is significantly larger than 7 µm. Kontos et al. [27] reported on the influence of the TNT layer thickness for the photocatalytic degradation of nitrogen oxide and found that 14 µm was the limit for UV light penetration and pollutant diffusion depth on TNT layers with a geometrical area of 10.7 cm^2, as the nitrogen oxide conversion did not increase for thicker TNT layers. This is in accordance with the results in this study.

Two distinct differences can be observed for the photocatalytic degradation of hexane and benzene. First of all, the conversion of hexane is higher for TNT layers of all thicknesses than the conversion of benzene, though the degradation of both compounds is initiated by an attack of ·OH radicals [43,44]. This can be explained by an easier oxidation of the aliphatic hexane than of the aromatic ring of benzene [6].

The second difference is that the photocatalytic degradation of hexane is very stable over the whole degradation time of three hours. On the other hand, for benzene a high degradation was observed at the beginning of the measurements, while very soon the conversion of benzene decreases. This phenomenon was already described for the photocatalytic degradation of benzene and toluene on TiO_2 nanoparticle layers [43,45] as well as for toluene for TNT layers [23]. ·OH radicals attack the aromatic ring of benzene, the resulting intermediate products are then further decomposed to CO_2. No intermediate product of benzene oxidation in the gaseous phase were found, on the other hand after

extraction from the used photocatalyst, traces of phenol, hydroquinone and 4-benzoquinone were observed [45]. Some of these intermediates (especially in the form of radicals) might also polymerize and then deposit on the TNT layer surface. Deposited hydrocarbon compounds may thus block the photocatalyst surface and the degradation rate decreases over time. However, as the conversion of benzene for all TNT layers reaches a steady value after about 3 hours of irradiation, it can be said that the presence of deposited intermediate products does not completely stop the photocatalytic degradation but only decrease it to ca. 50 % of the initial value (see Fig. 4B).

To get an insight on a presence of any species on TNT layers after the benzene photocatalytic experiments, post-mortem analyses were carried out. Since SEM did not reveal any obvious deposits on the surface of nanotubes, XPS analyses were carried out to analyze the carbon content on the top of the thickest TNT layer and the results were compared to a fresh TNT layer, i.e. not used for the photocatalytic degradation of benzene. The C 1s spectra are shown in Fig. S3, tables S5 and S6 summarize the elemental composition of the TNT layers as well as the different carbon species found. As can be seen, the composition of both TNT layers was almost identical, with a slight decrease in carbon species for the TNT layer used for benzene degradation. However, if carbon compounds were deposited on the TNT layer surface during benzene degradation, one would expect an increase in the carbon content. Interestingly, in case of the TNT layer used for benzene degradation, a very small signal at 280.2 eV could be assigned to titanium carbide [46]. However, the concentration of titanium carbide in the sample is too low to be confirmed by the Ti 2p Hi-res spectrum. Furthermore, Dronov et al. [47] found titanium carbide also within as-prepared TNT layers due to the decomposition of ethylene glycol during the anodization process. Thus, a direct conclusion on the deposition of carbon species on the TNT layer surface cannot be drawn from the XPS results.

Conclusions

In conclusion, the preparation of homogenous TNT layers with different thicknesses on the large scale was shown for the first time in this study. In particular the thickest prepared TNT layers show excellent performance for the degradation of hexane and benzene in the gas phase under ISO standards with an increase of conversion with the TNT layer thickness. However, a decrease in the benzene conversion was observed over time. Although in the literature this is explained by the deposition of carbon compounds stemming from the degradation of benzene on the surface of the TNT layers, no suspicious carbon species were observed by post-mortem SEM and XPS analyses of the TNT layers used in this study.

CRediT authorship contribution statement

Hanna Sopha: Conceptualization, Data curation, Formal analysis, Investigation, Methodology, Visualization, Writing – original draft, Writing – review & editing. **Michal Baudys:** Data curation, Formal analysis, Investigation, Writing – review & editing. **Ludek Hromadko:** Investigation, Visualization, Writing – review & editing. **Miloslav Lhotka:** Investigation, Writing – review & editing. **David Pavlinak:** Investigation, Writing – review & editing. **Josef Krysa:** Conceptualization, Methodology, Funding acquisition, Supervision, Writing – review & editing. **Jan M. Macak:** Conceptualization, Methodology, Funding acquisition, Project administration, Supervision, Writing – review & editing.

Declaration of Competing Interest

The authors declare that they have no known competing financial interests or personal relationships that could have appeared to influence the work reported in this paper.

Acknowledgments

The authors acknowledge the Czech Science Foundation (project 21-27243S) and the Ministry of Education, Youth and Sports of the Czech Republic (MEYS CR, project LM 2018103). The CzechNanoLab project LM2018110 funded by MEYS CR is gratefully acknowledged for the financial support of XPS investigations at CEITEC Nano Research Infrastructure.

Supplementary materials

Supplementary material associated with this article can be found, in the online version, at doi:10.1016/j.apmt.2022.101567.

References

[1] M.R. Hoffmann, S.T. Martin, W. Choi, D.W. Bahnemann, Environmental Applications of Semiconductor Photocatalysis, Chem. Rev. 95 (1995) 69–96, https://doi.org/10.1021/cr00033a004.
[2] A. Fujishima, T.N. Rao, D.A. Tryk, Titanium dioxide photocatalysis, J. Photochem. Photobiol. C Photochem. Rev. 1 (00) (2000) 1–21, https://doi.org/10.1016/S1389-5567, 00002-2.
[3] D.. Tryk, A. Fujishima, K. Honda, Recent topics in photoelectrochemistry: achievements and future prospects, Electrochim. Acta. 45 (00) (2000) 2363–2376, https://doi.org/10.1016/S0013-4686, 00337-6.
[4] O. Carp, C.L. Huisman, A. R, Photoinduced reactivity of titanium dioxide, Prog. Solid State Chem. 32 (2004) 33–177, https://doi.org/10.1016/j.progsolidstchem.2004.08.001.
[5] A.G. Kontos, A. Katsanaki, T. Maggos, V. Likodimos, A. Ghicov, D. Kim, J. Kunze, C. Vasilakos, P. Schmuki, P. Falaras, Photocatalytic degradation of gas pollutants on self-assembled titania nanotubes, Chem. Phys. Lett. 490 (2010) 58–62, https://doi.org/10.1016/j.cplett.2010.03.009.
[6] F. Moulis, J. Krýsa, Photocatalytic degradation of several VOCs (n-hexane, n-butyl acetate and toluene) on TiO2 layer in a closed-loop reactor, Catal. Today. 209 (2013) 153–158, https://doi.org/10.1016/j.cattod.2012.10.017.
[7] H. Sopha, M. Krbal, S. Ng, J. Prikryl, R. Zazpe, F.K. Yam, J.M. Macak, Highly efficient photoelectrochemical and photocatalytic anodic TiO2 nanotube layers with additional TiO2 coating, Appl. Mater. Today. 9 (2017) 104–110, https://doi.org/10.1016/j.apmt.2017.06.002.
[8] F. Moulis, J. Krýsa, Photocatalytic degradation of acetone and methanol in a flow-through photoreactor with immobilized TiO2, Res. Chem. Intermed. 41 (2015) 9233–9242, https://doi.org/10.1007/s11164-015-1989-2.
[9] A.K. Boulamanti, C.J. Philippopoulos, Photocatalytic degradation of C5-C7alkanes in the gas-phase, Atmos. Environ. 43 (2009) 3168–3174, https://doi.org/10.1016/j.atmosenv.2009.03.036.
[10] T.A. Kandiel, A. Feldhoff, L. Robben, R. Dillert, D.W. Bahnemann, Tailored Titanium Dioxide Nanomaterials: Anatase Nanoparticles and Brookite Nanorods as Highly Active Photocatalysts, Chem. Mater. 22 (2010) 2050–2060, https://doi.org/10.1021/cm903472p.
[11] M. Lafjah, A. Mayoufi, E. Schaal, F. Djafri, A. Benguedda, N. Keller, V. Keller, TiO2 nanorods for gas phase photocatalytic applications, Catal, Today 235 (2014) 193–200, https://doi.org/10.1016/j.cattod.2014.03.015.
[12] X. Wang, Z. Li, J. Shi, Y. Yu, One-Dimensional Titanium Dioxide Nanomaterials: Nanowires, Nanorods, and Nanobelts, Chem. Rev. 114 (2014) 9346–9384, https://doi.org/10.1021/cr400633s.
[13] Z. Wu, F. Dong, W. Zhao, H. Wang, Y. Liu, B. Guan, The fabrication and characterization of novel carbon doped TiO 2 nanotubes, nanowires and nanorods with high visible light photocatalytic activity, Nanotechnology 20 (2009), 235701, https://doi.org/10.1088/0957-4484/20/23/235701.
[14] Z. Wu, S. Guo, H. Wang, Y. Liu, Synthesis of immobilized TiO2 nanowires by anodic oxidation and their gas phase photocatalytic properties, Electrochem. Commun. 11 (2009) 1692–1695, https://doi.org/10.1016/j.elecom.2009.06.031.
[15] J.M. Macak, M. Zlamal, J. Krysa, P. Schmuki, Self-Organized TiO2 Nanotube Layers as Highly Efficient Photocatalysts, Small 3 (2007) 300–304, https://doi.org/10.1002/smll.200600426.
[16] M. Zlamal, J.M. Macak, P. Schmuki, J. Krysa, Electrochemically assisted photocatalysis on self-organized TiO2 nanotubes, Electrochem. Commun. 9 (2007) 2822–2826, https://doi.org/10.1016/j.elecom.2007.10.002.
[17] T. Kasuga, M. Hiramatsu, A. Hoson, T. Sekino, K. Niihara, Formation of Titanium Oxide Nanotube, Langmuir 14 (1998) 3160–3163, https://doi.org/10.1021/la9713816.
[18] K. Lee, A. Mazare, P. Schmuki, One-dimensional titanium dioxide nanomaterials: Nanotubes, Chem. Rev. 114 (2014) 9385–9454, https://doi.org/10.1021/cr500061m.
[19] J.M. Macak, H. Tsuchiya, L. Taveira, S. Aldabergerova, P. Schmuki, Smooth Anodic TiO2 Nanotubes, Angew. Chemie Int, Ed. 44 (2005) 7463–7465, https://doi.org/10.1002/anie.200502781.
[20] H. Sopha, T. Samoril, E. Palesch, L. Hromadko, R. Zazpe, D. Skoda, M. Urbanek, S. Ng, J. Prikryl, J.M. Macak, Ideally Hexagonally Ordered TiO2 Nanotube Arrays, ChemistryOpen 6 (2017) 480–483, https://doi.org/10.1002/open.201700108.

[21] D. Beketova, M. Motola, H. Sopha, J. Michalicka, V. Cicmancova, F. Dvorak, L. Hromadko, B. Frumarova, M. Stoica, J.M. Macak, One-Step Decoration of TiO2 Nanotubes with Fe3O4 Nanoparticles: Synthesis and Photocatalytic and Magnetic Properties, ACS Appl. Nano Mater. 3 (2020) 1553–1563, https://doi.org/10.1021/acsanm.9b02337.

[22] P. Mazierski, J. Nadolna, W. Lisowski, M.J. Winiarski, M. Gazda, M. Nischk, T. Klimczuk, A. Zaleska-Medynska, Effect of irradiation intensity and initial pollutant concentration on gas phase photocatalytic activity of TiO2 nanotube arrays, Catal. Today. 284 (2017) 19–26, https://doi.org/10.1016/j.cattod.2016.09.004.

[23] M. Nischk, P. Mazierski, M. Gazda, A. Zaleska, Ordered TiO2 nanotubes: The effect of preparation parameters on the photocatalytic activity in air purification process, Appl. Catal. B Environ. 144 (2014) 674–685, https://doi.org/10.1016/j.apcatb.2013.07.041.

[24] V. Jaeger, W. Wilson V, Ravi) Subramanian, Photodegradation of methyl orange and 2,3-butanedione on titanium-dioxide nanotube arrays efficiently synthesized on titanium coils, Appl. Catal. B Environ. 110 (2011) 6–13, https://doi.org/10.1016/j.apcatb.2011.08.005.

[25] H. Sopha, M. Baudys, M. Krbal, R. Zazpe, J. Prikryl, J. Krysa, J.M. Macak, Scaling up anodic TiO2 nanotube layers for gas phase photocatalysis, Electrochem. Commun. 97 (2018) 91–95, https://doi.org/10.1016/j.elecom.2018.10.025.

[26] M. Motola, M. Baudys, R. Zazpe, M. Krbal, J. Michalička, J. Rodriguez-Pereira, D. Pavliňák, J. Přikryl, L. Hromádko, H. Sopha, J. Krýsa, J.M. Macak, 2D MoS 2 nanosheets on 1D anodic TiO 2 nanotube layers: an efficient co-catalyst for liquid and gas phase photocatalysis, Nanoscale 11 (2019) 23126–23131, https://doi.org/10.1039/C9NR08753B.

[27] A.G. Kontos, A. Katsanaki, V. Likodimos, T. Maggos, D. Kim, C. Vasilakos, D. D. Dionysiou, P. Schmuki, P. Falaras, Continuous flow photocatalytic oxidation of nitrogen oxides over anodized nanotubular titania films, Chem. Eng. J 179 (2012) 151–157, https://doi.org/10.1016/j.cej.2011.10.072.

[28] M. Motola, L. Satrapinsky, T. Roch, Š. Jan, J. Kupčík, M. Klementová, M. Jakubičková, F. Peterka, G. Plesch, Anatase TiO2 nanotube arrays and titania films on titanium mesh for photocatalytic NOX removal and water cleaning, Catal. Today. 287 (2017) 59–64, https://doi.org/10.1016/j.cattod.2016.10.011.

[29] Z. Liu, X. Zhang, S. Nishimoto, T. Murakami, A. Fujishima, Efficient Photocatalytic Degradation of Gaseous Acetaldehyde by Highly Ordered TiO2 Nanotube Arrays, Environ. Sci. Technol. 42 (2008) 8547–8551, https://doi.org/10.1021/es8016842.

[30] M. Hattori, K. Noda, K. Kobayashi, K. Matsushige, Gas phase photocatalytic decomposition of alcohols with titanium dioxide nanotube arrays in high vacuum, Phys. Status Solidi. 8 (2011) 549–551, https://doi.org/10.1002/pssc.201000455.

[31] I.M. Mehedi, M.F. Hossain, T. Takahashi, M.S. Islam, Nano-structural variation of highly aligned anodic Titania nanotube arrays for gas phase photocatalytic application, J. Photochem. Photobiol. A Chem. 335 (2017) 200–210, https://doi.org/10.1016/j.jphotochem.2016.11.019.

[32] N. Sato, A THEORY FOR BREAKDOWN OF ANODIC OXIDE FILMS ON METALS*, Electrochim. Acta. 16 (1971) 1683–1692.

[33] M. Alijani, H. Sopha, S. Ng, J.M. Macak, High aspect ratio TiO2 nanotube layers obtained in a very short anodization time, Electrochim. Acta. 376 (2021), 138080, https://doi.org/10.1016/j.electacta.2021.138080.

[34] J. Lincho, J. Gomes, M. Kobylanski, B. Bajorowicz, A. Zaleska-Medynska, R. C. Martins, TiO2 nanotube catalysts for parabens mixture degradation by photocatalysis and ozone-based technologies, Process Saf. Environ. Prot. 152 (2021) 601–613, https://doi.org/10.1016/j.psep.2021.06.044.

[35] E. Mena, M.J. Martín de Vidales, S. Mesones, J. Marugán, Influence of anodization mode on the morphology and photocatalytic activity of TiO2-NTs array large size electrodes, Catal. Today. 313 (2018) 33–39, https://doi.org/10.1016/j.cattod.2017.12.036.

[36] C. Xiang, L. Sun, Y. Wang, G. Wang, X. Zhao, S. Zhang, Large-Scale, Uniform, and Superhydrophobic Titania Nanotubes at the Inner Surface of 1000 mm Long Titanium Tubes, J. Phys. Chem. C. 121 (2017) 15448–15455, https://doi.org/10.1021/acs.jpcc.7b03124.

[37] H. Kim, D. Kim, W. Kim, Y.-C. Ha, S.-J. Sim, S. Kim, W. Choi, Anodic TiO2 nanotube layer directly formed on the inner surface of Ti pipe for a tubular photocatalytic reactor, Appl. Catal. A Gen. 521 (2016) 174–181, https://doi.org/10.1016/j.apcata.2015.10.039.

[38] J.M. Macak, P. Schmuki, Anodic growth of self-organized anodic TiO2 nanotubes in viscous electrolytes, Electrochim. Acta. 52 (2006) 1258–1264, https://doi.org/10.1016/j.electacta.2006.07.021.

[39] H. Sopha, L. Hromadko, K. Nechvilova, J.M. Macak, Effect of electrolyte age and potential changes on the morphology of TiO2 nanotubes, J. Electroanal. Chem. 759 (2015) 122–128, https://doi.org/10.1016/j.jelechem.2015.11.002.

[40] J.I. Langford, A.J.C. Wilson, Scherrer after sixty years: A survey and some new results in the determination of crystallite size, J. Appl. Crystallogr. 11 (1978) 102–113, https://doi.org/10.1107/S0021889878012844.

[41] J. Zita, J. Krýsa, U. Černigoj, U. Lavrenčič-Štangar, J. Jirkovský, J. Rathouský, Photocatalytic properties of different TiO2 thin films of various porosity and titania loading, Catal. Today. 161 (2011) 29–34, https://doi.org/10.1016/j.cattod.2010.11.084.

[42] K. Zhu, N.R. Neale, A. Miedaner, A.J. Frank, Enhanced Charge-Collection Efficiencies and Light Scattering in Dye-Sensitized Solar Cells Using Oriented TiO2 Nanotubes Arrays, Nano Lett 7 (2007) 69–74, https://doi.org/10.1021/nl062000o.

[43] H. Einaga, S. Futamura, T. Ibusuki, Heterogeneous photocatalytic oxidation of benzene, toluene, cyclohexene and cyclohexane in humidified air: comparison of decomposition behavior on photoirradiated TiO2 catalyst, Appl. Catal. B Environ. 38 (02) (2002) 215–225, https://doi.org/10.1016/S0926-3373, 00056-5.

[44] V. Augugliaro, M. Bellardita, V. Loddo, G. Palmisano, L. Palmisano, S. Yurdakal, Overview on oxidation mechanisms of organic compounds by TiO2 in heterogeneous photocatalysis, "Journal Photochem. Photobiol. C Photochem. Rev 13 (2012) 224–245, https://doi.org/10.1016/j.jphotochemrev.2012.04.003.

[45] O. D'Hennezel, P. Pichat, D.F. Ollis, Benzene and toluene gas-phase photocatalytic degradation over H2O and HCL pretreated TiO2: by-products and mechanisms, J. Photochem. Photobiol. A Chem. 118 (98) (1998) 197–204, https://doi.org/10.1016/S1010-6030, 00366-9.

[46] J.E. Krzanowski, R.E. Leuchtner, Chemical, Mechanical, and Tribological Properties of Pulsed-Laser-Deposited Titanium Carbide and Vanadium Carbide, J. Am. Ceram. Soc. 80 (1997) 1277–1280, https://doi.org/10.1111/j.1151-2916.1997.tb02976.x.

[47] A. Dronov, I. Gavrilin, E. Kirilenko, D. Dronova, S. Gavrilov, Investigation of anodic TiO2 nanotube composition with high spatial resolution AES and ToF SIMS, Appl. Surf. Sci. 434 (2018) 148–154, https://doi.org/10.1016/j.apsusc.2017.10.132.